Title

Molecular Nature of Mineral-Organic Associations within Redox-Active Mountainous Floodplain Sediments

Journal

ACS Earth and Space Chemistry, 7(9)

ISSN

2472-3452

Authors

Anderson, Cam G
Goebel, Genevieve M
Tfaily, Malak M
et al.

Publication Date

2023-09-21

DOI

10.1021/acsearthspacechem.3c00037

Molecular nature of mineral-organic associations within redox-active mountainous floodplain sediments

Cam G. Anderson[1], Genevieve M. Goebel[1#], Malak M. Tfaily[2], Patricia M. Fox[3], Peter S. Nico[3], Scott Fendorf[4], Marco Keiluweit[5]*

[1]School of Earth and Sustainability, University of Massachusetts Amherst, Amherst, MA 01003 USA

[2]Department of Environmental Science, University of Arizona, Tucson, AZ 85721 USA

[3]Earth and Environmental Sciences, Lawrence Berkeley National Laboratory, Berkeley, CA 94720 USA

[4]Earth System Science, Stanford University, Stanford, CA 94305 USA

[5]Institute of Earth Surface Dynamics, University of Lausanne, 1015 Lausanne, Switzerland

***Corresponding Author:** Marco Keiluweit (marco.keiluweit@unil.ch)

Present Addresses

#Department of Biological Sciences, Dartmouth College, Hanover, NH 03755 USA

Keywords: Soil organic carbon, Floodplains, Redox gradients, Mineral-organic associations, Climate Change

Abstract

Floodplains are important terrestrial-aquatic interfaces that acts as hotspots of organic carbon (OC) cycling, regulating ecosystem carbon storage as well as export to riverine systems. Within floodplain sediments, regular flooding and textural gradients interact to create dynamic redox conditions. While anaerobic protection of OC upon burial is a well-recognized carbon storage mechanism in redox-active floodplain sediments, the impact of protective mineral-organic associations is relatively unknown. Here, we determined the quantitative importance and chemical composition of mineral-organic associations along well-defined redox gradients emerging from textural variations and depth within meander sediments of the subalpine East River watershed (Gothic, CO). We characterized mineral-organic associations using a combination of sequential extractions, physical fractionation, and high-resolution mass spectrometry. Across the meander, we found that mineral-associated OC constitutes a meaningful fraction of total OC, and that extractable iron (Fe) and aluminum (Al) phases and high-density isolates were strongly correlated with total OC content, suggesting that mineral-organic associations are quantitatively important for floodplain sediment OC protection. Our mass spectrometry results showed OC associated with increasingly ordered Fe and Al phases are relatively enriched in low-molecular weight, oxidized, aromatic compounds. To our surprise, however, total OC content showed weak or no correlation with indicators of anaerobic protection, such as relatively bioavailable OC pools (water-extractable and particulate OC) or the molecular weight and oxidation state of OC. Overall, this work highlights that mineral protection of OC bound to reactive mineral phases – in addition to anaerobic protection – can play a quantitatively important role in controlling soil carbon storage in redox-active floodplain sediments.

Introduction

Floodplains are important terrestrial-aquatic interfaces that can act as carbon sinks or sources, regulating ecosystem carbon storage within and export to riverine systems [1,2]. Globally, floodplain ecosystems are estimated to account for up to 8% of global soil organic carbon (OC) storage, despite covering only 1% of the land area surface [3]. Each year, 0.25 Pg OC are transferred from floodplain to riverine systems, and eventually exported to oceans [4]. OC stored within floodplains is increasingly precarious in the Anthropocene, as climate change and human alteration affect the timing and magnitude of flooding cycles [5]. These changes are particularly pronounced in headwater systems of the mountainous western United States, with a current megadrought [6] foreshadowing further predicted declines in snow water equivalent [7]. To predict the impact of these drastic hydrological changes on OC retention and loss within floodplain sediments, specifically those in mountainous systems, a mechanistic understanding of the rate-controlling mechanisms is critical.

Seasonal flooding and the resulting depositional environment create a mosaic of floodplain sediments with varying characteristics and propensities to sequester OC. The storage of sediment OC is temporally and spatially heterogeneous, depending on factors including grain size distribution, soil moisture dynamics, and biogeochemical processes [8,9]. For example, seasonal flooding events result in particle sorting and accumulation of fine sediment, resulting in distinct textural patterns across floodplain meanders and with sediment depth [3]. While sediment burial is a major factor governing OC storage in floodplains [1,10–12], the mechanisms governing floodplain OC storage, and how burial interacts with texture, moisture, and biogeochemical gradients, are poorly understood.

In depositional floodplain sediments, textural gradients give rise to spatially dynamic redox conditions. Reducing conditions dominate both when sediments are saturated during flooding and in fine-textured sediments. It is commonly assumed that oxygen limitations experienced under reducing conditions are primarily responsible for OC preservation in the floodplain [13–15]. The absence of oxygen imposes both kinetic and thermodynamic constraints on microbial activity and can limit depolymerization and respiration of organic compounds [16,17], resulting in anaerobic protection of OC in the floodplain. Under anaerobic conditions, the activity of oxidative enzymes capable of catalyzing depolymerization reactions is restricted [18], causing the preservation of complex particulate organic carbon (POC) [17]. Additionally, the degree of microbial respiration in anaerobic environments is not just dependent on the energetics of available terminal electron acceptors (e.g., Fe(III) or sulfate), but also on the oxidation state of the electron donor, i.e., the organic substrate utilized by microbes [19]. Boye et al. [19] found that in floodplain sediments, reduced organic compounds with nominal oxidation state of carbon values (NOSC) below a thermodynamic threshold that makes microbial respiration unfavorable are selectively preserved. The influence of such kinetic and thermodynamic constraints, here termed anaerobic protection, will likely vary along spatial redox gradients within floodplain environments, which can form within microsites, along textural transitions, or along the capillary fringe [16,18,20].

While anaerobic protection of OC within sediments has received widespread attention [16,19,21,22], it is less clear how reactive metals influence OC preservation within floodplain environments. Associations with reactive minerals effectively protect organic compounds from microbial oxidation [23] and represent an important C storage mechanism in upland soil systems [21,24,25]. Iron (Fe) and aluminum (Al) (oxy)(hydr)oxides (in the following abbreviated as “oxides”)

are particularly important for the formation of mineral-organic associations [26,27], especially in humid and/or redox-active systems [28–30]. This contrasts with relatively arid and alkaline systems, where organic complexes with calcium (Ca) can be an important OC stabilization mechanism [30]. Although the abundance of reactive Fe/Al/Ca phases can constitute a significant component of the mineral matrix in floodplain sediments [8,31,32], their quantitative importance for OC retention has not been considered.

The importance of reactive metals in driving OC cycling likely shifts depending on the redox regime, because Fe, unlike Al and Ca, is redox-active [33–35]. The stability of Fe-OC associations is impacted by redox oscillations: reducing conditions can lead to their disruption through reductive dissolution of Fe oxides and subsequent leaching [21]; conversely, oxic conditions promote the formation of protective Fe-OC associations through precipitation reactions [36–39]. In floodplains, it is expected that spatiotemporal variations in oxygen availability (and thus redox) as imposed by water table depth or textural gradients cause local variation in Fe reduction and oxidation, likely regulating the relative importance of Fe-OC associations [12,31] as compared to protective associations between OC and Al or Ca [30,35,40]. This is in contrast to organic soils, where anaerobic protection can combine with low pH in regulating OC storage, where O_2 limitation, low pH, and high phenol concentrations combine to limit organic matter decomposition [41, 42].

In mineral-rich sediments, redox fluctuations alter both the degree of microbial OC transformation and mineral reactivity. Consequently, such fluctuations dictate the chemical nature of mineral-associated OC (MAOC) that might form. For example, plant-derived aromatic OC preferentially binds to increasing short-range order mineral content [43–45] in tropical and volcanic soils, which may be stabilized on Fe oxide surfaces during redox fluctuations [38].

However, because redox fluctuations affect the crystallinity of Fe oxides [38,46,47], we expect that MAOC composition varies in redox-active soils. For example, in humid tropical soils which undergo frequent redox oscillations, Coward et al. [43] found that varying Fe mineral phases, as determined by sequential extraction, associated with unique OC compounds. Together, these observations suggest that the chemical composition of mineral-organic associations in floodplains will vary with redox regime.

In this study, we determined the quantitative importance and chemical composition of mineral-organic associations within redox-active subalpine floodplain sediments. To assess the impact of redox conditions on the characteristics of mineral-organic associations, we sampled along well-defined redox gradients emerging from textural variations and depth within an active floodplain meander of the East River (Gothic, CO). This study area is representative of headwater catchments in the Upper Colorado Basin, an area that supplies water resources to a large portion of the Western United States [48]. We quantified the amount of mineral-associated OC (MAOC) using physical density fractionation and chemical extractions. To characterize the chemical composition of MAOC, we used a combination of selective dissolution with subsequent analysis by Fourier-transform ion cyclotron resonance mass spectrometry (FT-ICR-MS). Finally, we compared abundance and chemical composition of bioavailable OC and MAOC to infer the relative importance of mineral protection versus anaerobic protection on floodplain C cycling. We hypothesized that the chemical composition of mineral-organic associations is dictated by changes in mineral reactivity across redox gradients, and that the quantitative importance of MAOC will be lowest within more reducing environments.

Materials and Methods

134

135 **Field site description**. We established a sampling transect across an active meander of the East
136 River floodplain (Gothic, CO; Fig. 1). This location was chosen as it is a representative meander
137 of the subalpine region of the East River watershed, and has been studied extensively in terms of
138 geochemical dynamics [49,50] and carbon chemistry [51]. Sediment profiles across the transect
139 consisted of fine-grained material (< 2 mm) overlaying more coarse-grained alluvium, all
140 underlain by Mancos shale [51]. Floodplain vegetation included dwarf shrubs (e.g., American
141 dwarf birch and mountain willow), potentilla, and grasses [52]. Water table depth was calculated
142 using pressure transducers (Hobo U20L-04) installed along the sampling transect [53]: over the
143 course of seasonal flooding, the water table declined by 0.4 m at the near river position and 0.9
144 m at the mid-meander position (Table S1). Measurements of soil moisture (Acclima TDR-315L)
145 and redox potential (in-house platinum-tipped electrodes) were taken at the same sampling
146 locations and depths in 2019, a year that experienced similar levels of river discharge and
147 subsequent flooding as 2017 (Fig. S1).

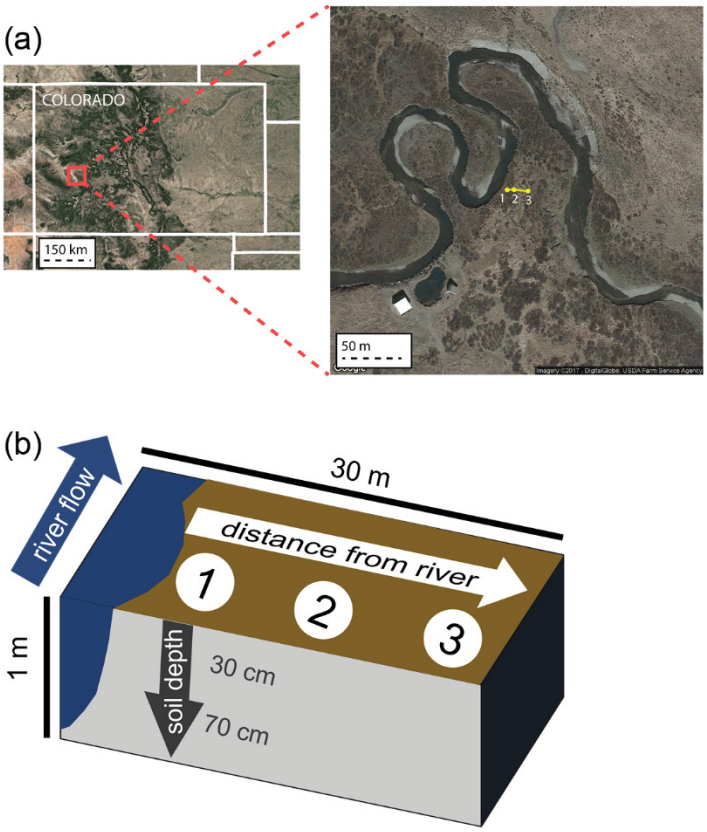

Figure 1: (a) Location of East River sampling transect in Colorado, and (b) schematic of the transect across the meander with distance from the river (positions 1, 2, and 3 representing near river, intermediate, and mid-meander positions, respectively) and sampled depths (30 cm and 70 cm). East River discharge values and corresponding sediment moisture and redox values are provided in Supporting Information (Fig. S1, Table S1).

Sediment sampling. We collected sediment samples in triplicate in June 2017 at three positions along the sampling transect, at shallow (30 cm) and deep depths (70 cm) (Fig. 1, Table S2); these depths were chosen based on visual assessment of sediment redoximorphic features during field sampling. Sediments were air-dried and sieved to 2 mm. Sediments across the transect dry out to 27-59% volumetric water content upon drainage in September (Table S1); thus, precipitation of redox-active metal phases may have occurred during sample processes and the data reported here likely represent the state of mineral-organic associations present within the sediments during fully drained, oxic periods spanning from mid-summer to the following spring. No unexpected or

unusually high safety hazards were encountered in the sampling and subsequent analysis of sediment samples.

Bulk sediment characterization. We determined total sediment carbon and nitrogen in triplicate using an ECS 4010 CHNS-O elemental analyzer (Costech Analytical Technologies, Inc., Valencia, CA, USA). We measured total metals (Fe, Al, Ca, Si, etc.) on finely ground samples using X-ray fluorescence (Spectro Xepos HE XRF Spectrometer). We determined sediment texture after loss on ignition to remove organic matter (4 h at 550 C) by a laser diffraction particle size analyzer (Beckman Coulter LS 13 320, Indianapolis, IN). We estimated root biomass by picking out coarse roots from air dried sediments. Analytical error was orders of magnitude lower than the variance among biological replicates, and thus only standard error of the means of biological replicates are reported.

Density fractionation. To isolate organic matter of decreasing bioavailability (e.g., particulate to mineral-associated organic matter), we used a density fractionation procedure modified from the literature[54,55]. Briefly, two sodium polytungstate (SPT) solutions were prepared in DI water at the following densities: 1.6 g cm^3 and 2.2 g cm^3 (solutions #1 and #2, respectively). Particulate organic matter was determined by adding and gently vortexing 30 ml of solution #1 and 7.5 g of sediment, shaking for 2 h at low speed, and centrifuging for 1 h at 1000 x g. The supernatant was filtered (0.8 μm, Millipore), rinsed thoroughly with DI water to remove excess SPT, and the filter was oven-dried at 60 C and weighed to determine the amount of particulate organic matter. To determine the intermediate density fraction (> 1.6 and < 2.2 cm^3), 30 ml of solution #2 was added to the remaining sediment pellet, and the above steps were repeated. The final density fraction (> 2.2 g cm^3) was determined by thoroughly cleaning the remaining sediment pellet with DI water. 30 ml of DI water was added and vortexed until the pellet was suspended, then

centrifuged for 1 h at 2000 x g. The supernatant was removed, and this process was repeated three times. The dry mass of the remaining sediment pellet was recorded. The intermediate and heavy fractions together comprised the MAOC pool. We determined carbon and nitrogen content of density fractions in triplicate as described above for bulk sediment.

Sequential extractions. To selectively dissolve mineral phases of varying degrees of order and their associated organic matter, sediments were extracted sequentially with four reagents [56–58]. After each extraction, the supernatant was filtered using 0.22 μm filters (Sigma-Aldrich). Briefly, 0.33 g sediment was extracted with 10 ml deionized (DI) water to extract bioavailable phases of minerals and organic matter (shaken 2 h at 200 rpm, centrifuged 20 min at 510 x g); this extraction represented water-extractable organic carbon (WEOC). The same pellet was then extracted with 10 ml of 0.1 M sodium pyrophosphate to target amorphous metal-organic complexes[57,59] (shaken 16 h at 200 rpm, centrifuged 1 h at 4000 x g) and combined with the filtered extract of a 6.7 ml DI water rinse (shaken 2 h at 200 rpm, centrifuged 1 h at 4000 x g). Then, 10 ml of 0.5 M hydrochloric acid (HCl) was added to the remaining pellet to target short-range order phases [56] (shaken 4 h at 200 rpm, centrifuged 20 min 4000 x g) and combined with the filtered extract of a 6.7 ml DI water rinse (shaken 2 h at 200 rpm, centrifuged 20 min at 510 x g). Lastly, 10 ml of 0.049 M sodium dithionite was added to the pellet to target total reducible oxide phases [58] (shaken 16 h at 200 rpm, centrifuged 20 min at 510 x g) and combined with the filtered extract of a 6.7 ml of 0.05 M HCl rinse (shaken 1 h at 200 rpm, centrifuged 20 min at 510 x g).

Metal and TOC analysis of sequential extractions. Extracts were analyzed for metals using Microwave Plasma-Atomic Emission Spectrometry (Agilent, Santa Clara, CA), diluting to a final

concentration of 2% nitric acid. Extracts were analyzed for total organic carbon using a TOC-L Analyzer (Shimadzu, Kyoto, Japan), diluting in DI water.

Fourier-transform ion cyclotron resonance mass spectrometry (FT-ICR-MS) analysis of sequential extractions. Extracts were analyzed for organic matter composition using a 12 Tesla Bruker SolariX FTICR spectrometer located at the Environmental Molecular Science Laboratory in Richland, WA. Samples were first desalted and concentrated using solid phase extraction[60] with bond elute PPL cartridges. The analyte was eluted from the PPL cartridge in HPLC grade methanol and introduced directly to a standard Bruker electrospray ionization source operating in negative mode. The instrument was externally calibrated weekly to a mass accuracy of < 0.1 ppm using a tuning solution from Agilent. The ion accumulation time varied to account for differences in C concentration between samples. A Suwannee River Fulvic Acid standard, obtained from the International Humic Substance Society, was used as a control to monitor potential carryover from one sample to another and ensure instrument stability in day-to-day operation. The instrument was flushed between samples using a mixture of Milli-Q water and HPLC grade methanol. One hundred and forty-four individual scans were averaged for each sample and internally calibrated using OM homologous series separated by 14 Da (-CH_2 groups). The mass measurement accuracy was < 1 ppm for singly charged ions across a broad mass-over-charge (m/z) range (i.e., 100 < m/z < 1100). The mass resolution was 350,000 at 339.112 Da. BrukerDaltonik data analysis software (version 4.2) was used to convert raw spectra to a list of m/z values applying FT-MS peak picker module with a signal-to-noise ratio threshold of 7 and absolute intensity threshold of 100. Formularity software[61] was used to assign chemical formulae based on the criteria previously described[62]. Peaks were filtered to only include masses between 200 < m/z < 900. Compounds were grouped into molecular classes (e.g., lipid-, protein-,

carbohydrate-, lignin-, tannin-, condensed aromatic-like) based on C, H, and O for H/C and O/C ranges according to previous literature[63] . Each assigned molecular formula was used to calculate the nominal oxidation state of C (NOSC), double bond equivalence (DBE), and aromaticity index (AI) as in previous work [21].

Statistical analysis. All statistical analyses were performed using R version 4.2.2 [64]. We used Shapiro-Wilk and Levene's tests to assess normality and equality of variances for all data. Parametric tests were used in cases in which data met assumptions for normality. To test our hypotheses, we grouped by sediment depth and assessed differences among meander positions or extractions using analysis of variance (ANOVA), combined with Tukey's honestly significant difference *post hoc* test ($\alpha = 0.05$ indicates significant differences), using the R package *agricolae* [65]. Specifically, we compared values within surface (30 cm) and deep (70 cm) sediments across the lateral meander transect from near river to mid-meander locations (Fig. 1) and among extractions. We performed linear regressions to determine relationships between sediment C and sediment properties ($\alpha = 0.05$ indicates significant differences).

Results and Discussion

Physical and chemical characteristics of meander sediments dictate redox regime

Along the meander transect and with depth, spatial variations in sediment texture, moisture, and root C inputs resulted in pronounced redox gradients. Clay and silt content was 53% greater in

shallow (30 cm, 89.6%) than deep sediments (70 cm, 58.7%), and in deep sediments the clay and silt content was 105% greater at the meander center (79.6%) compared to the near river position (39.9%) (Table 1). Due to the finer texture in the meander center, the moisture content remained higher across both depths (65-67% volumetric water content, VWC) compared to the near river position (43%- 47% VWC) during early season flooding (Table S1). As a result of these texture and moisture patterns during flooding, the mid-meander position experienced lower redox potentials at both depths (-180 to 240 mV), while the coarse textured and well-drained near-river position remained relatively oxic (9 to 355 mV, Table S1). Root biomass, used here as a proxy for root C inputs, decreased by 85% from shallow (1510.7 mg) to deep sediments (220.3 mg), with no significant differences among the meander positions (Table 1). Total metals varied significantly across the meander, but not with depth: total Fe in the mid-meander position (3.9%) was 22% greater than the near river position (3.2%), while total Ca in the near river position (2.3%) was 156% higher versus the mid-meander position (0.9%). There were no significant trends in total Al. Sediment pH was 11% greater in the near river position (7.9) than mid-meander position (7.1), and 13% greater in the deep (7.8) compared to shallow horizons (6.9) (Table 1).

Table 1: Physical and chemical characteristics of meander sediments (mean +/- standard error), across meander position and depth. Bulk metals included iron (Fe), aluminum (Al), and silicon (Si). Density isolates included particulate organic carbon (POC) and mineral-associated organic carbon (MAOC).

Position	Depth (cm)	Sand (%)	Silt + clay (%)	pH	Root biomass (mg)	Bulk Fe (%)	Bulk Al (%)	Bulk Ca (%)	Bulk Si (%)	POC (mmol C / g)	MAOC (mmol C / g)
Near river	30	13.9 ± 0.8	86.1 ± 0.8	7.3 ± 0.02	2011 ± 932	3.07 ± 0.08	4.97 ± 0.11	2.22 ± 0.08	23.91 ± 0.49	4.28 ± 1.22	3.88 ± 0.59
	70	61.1 ± 6.0	38.9 ± 6.0	8.3 ± 0.08	309 ± 183	3.34 ± 0.18	5.60 ± 0.04	2.42 ± 0.07	26.55 ± 0.09	2.44 ± 0.29	1.24 ± 0.21
Intermediate	30	8.7 ± 1.1	91.3 ± 1.1	6.5 ± 0.03	460 ± 84	3.25 ± 0.09	5.29 ± 0.08	1.25 ± 0.10	24.43 ± 0.57	3.41 ± 1.23	4.81 ± 0.53
	70	42.3 ± 9.1	57.7 ± 9.1	7.7 ± 0.10	128 ± 71	3.32 ± 0.12	5.72 ± 0.09	1.58 ± 0.12	26.89 ± 0.40	1.45 ± 0.02	1.18 ± 0.10
Mid-meander	30	8.6 ± 0.3	91.4 ± 0.3	6.7 ± 0.11	2062 ± 1705	3.75 ± 0.07	5.56 ± 0.11	1.01 ± 0.08	25.77 ± 0.55	3.40 ± 0.51	3.66 ± 0.73
	70	20.4 ± 2.0	79.6 ± 2.0	7.5 ± 0.02	223 ± 76	4.15 ± 0.27	5.30 ± 0.43	0.71 ± 0.01	25.55 ± 1.47	0.95 ± 0.12	0.93 ± 0.06

Mineral-associated carbon pools vary spatially across the meander

Total OC, as well as POC, MAOC, and root biomass, were significantly greater in the surface compared to deep sediments (Fig. 2a, Table 1, $p < 0.05$). No significant changes in root biomass were observed across the floodplain meander (Table 1). However, contrary to our original hypothesis, total sediment C and POC significantly declined towards the finer textured, more reducing meander center, a trend particularly pronounced with depth (Fig. 2a, $p < 0.05$). Burial of POC and subsequent kinetic and thermodynamic protection due to limited oxidative depolymerization are common mechanisms of floodplain sediment C storage [1,10–12,18]. If such protection mechanisms were dominant, we would expect the highest sediment OC and POC contributions in the more reducing meander center; however, we find both pools lowest at the meander center compared to the relatively oxic near-river position. This finding suggests that kinetic and thermodynamic constraints do not solely explain the patterns of C storage across the meander.

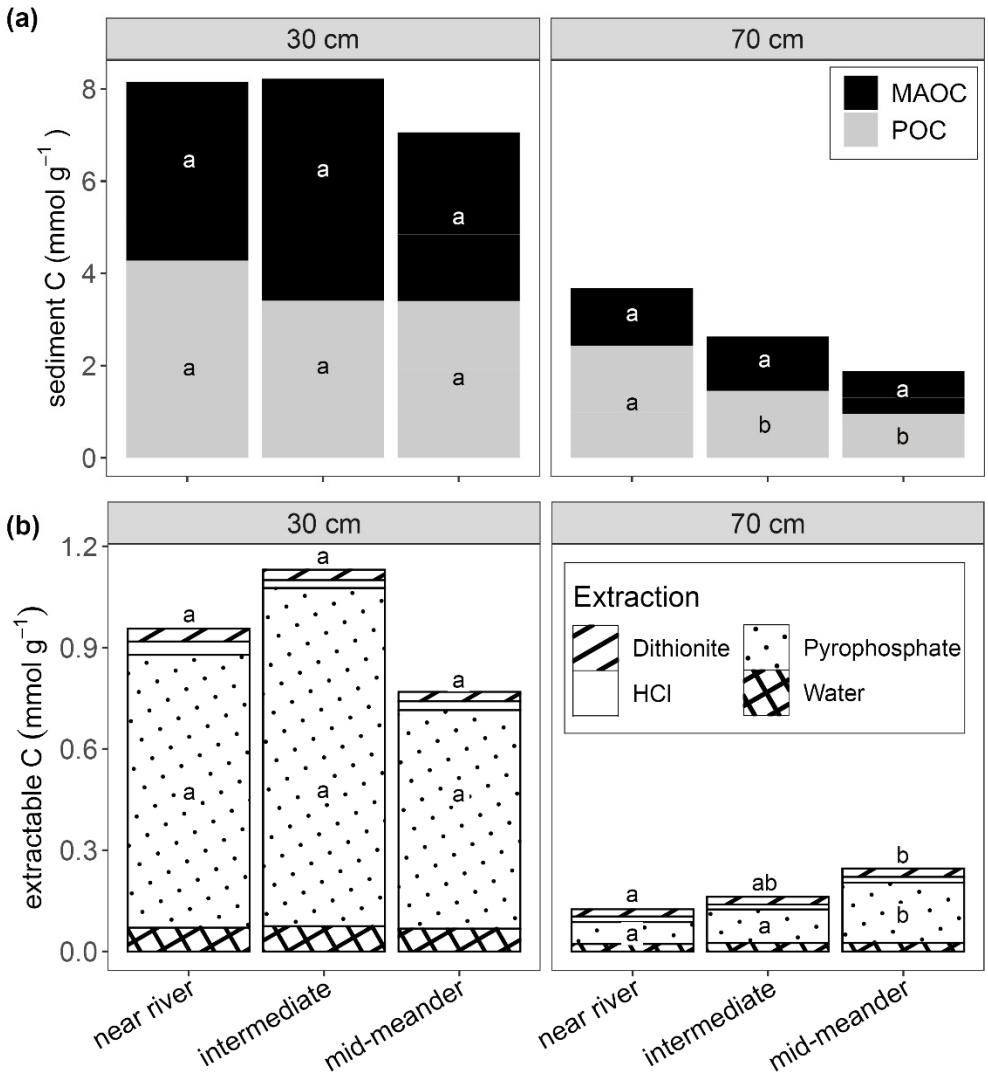

Figure 2: Sediment OC in shallow (30 cm) and deep (70 cm) sediment, across the floodplain meander in (a) bulk pools, separated by mineral-associated organic carbon (MAOC) and particulate organic carbon (POC) (denoted by black and gray shading, respectively), and (b) extractable pools, separated by extraction (denoted by pattern fills). Units for both panels are mmol C per g sediment. Letter designations are Tukey's honestly significant difference test results ($p < 0.05$) based on differences along the meander in each depth: differences in MAOC and POC in panel (a), and differences in total extractable OC and pyrophosphate-extractable OC in panel (b). Mean and standard errors are reported in Table 1 for bulk pools, and in Table S3 for extractable OC.

Our proxies for MAOC better predict the spatial distribution of total OC across the meander than POC. Notably, in deep sediments, the relative contribution of MAOC (isolated by density fractionation) compared to POC increased by 38% towards the center of the meander (Fig. 2a, $p < 0.05$). Similarly, the total amount of extractable OC (sum of water, pyrophosphate,

HCl, and dithionite extractable OC) increased in the deep sediment at the mid-meander position (Fig. 2b, $p < 0.05$). Both independent lines of evidence indicate that mineral protection becomes relatively more important towards the finer-textured, more reducing meander center, and especially in deep sediments. This finding is counter to our expectation that mineral protection, particularly via bonds to Fe oxides, would decrease towards the more reduced deeper sediments of the meander center due to microbial Fe reduction [31]. Rather, this suggests that mineral-organic associations play an important role in C storage, even in temporarily reduced locations of the floodplain meander.

Sequential extractions further highlight the importance of Fe and Al oxides in driving patterns of OC accumulation across the meander. Along the floodplain meander, total extractable Fe and Al concentrations as well as MAOC isolated by density fractionation strongly and significantly correlated with sediment C content (Fig. 3, $p < 0.05$). Extractable Ca, which can effectively protect OC in alkaline soils (Rasmussen et al. 2018), only significantly correlated with OC content in the more alkaline deep soils (Fig. S2a, $p < 0.05$). In contrast, clay content did not significantly correlate with total sediment C content (Fig. S2b). Our results therefore suggest that mineral protection of OC in our floodplain sediments is due to pedogenic (extractable) Fe and Al oxides, and Ca-organic complexes at depth, rather than phyllosilicates.

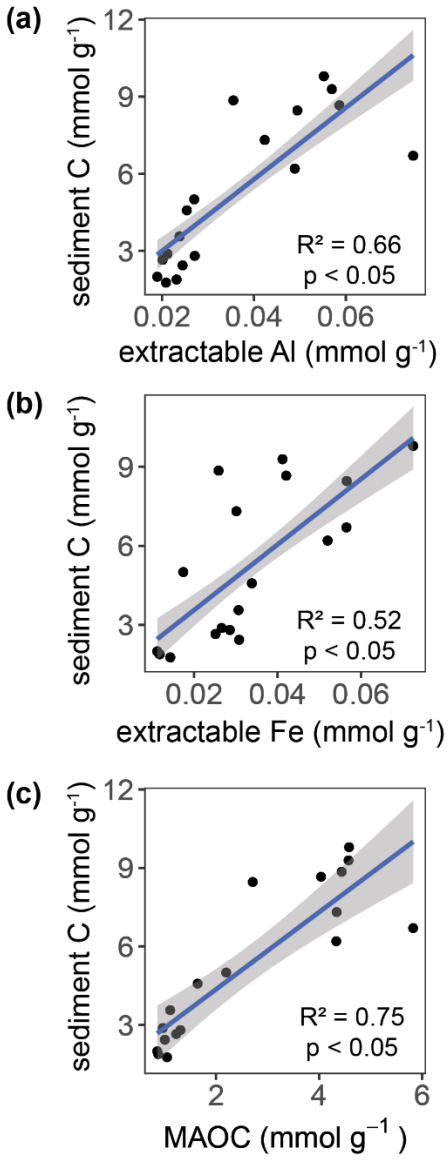

Figure 3: Correlations between sediment OC and (a) extractable aluminum (Al), (b) extractable iron (Fe), and (b) mineral-associated organic carbon (MAOC). Units for all panels are mmol C per g sediment. The blue line is the linear regression and statistics are provided, including the R^2 and p-value for model significance.

Total extractable OC was higher in surface compared to deep sediments and increased towards the meander center in the deep sediments (Fig. 2b, $p < 0.05$). Pyrophosphate extracted significantly more OC than other extractants across both depths and all meander positions (Fig. 2b, $p < 0.05$). Comparison of the OC pools extracted during selective dissolutions shows that in deep sediments, pyrophosphate-extractable OC is principally responsible for the significant

increase in total extractable OC towards the meander center (Fig. 2b, $p < 0.05$). This increase in the contribution of pyrophosphate-extractable OC towards the more reducing meander center suggests protection of C within metal-organic complexes[57,66], although this pool might include nanoparticulate metal oxide phases [67] and base-extractable organic matter [57]. Together, these results show that OC associated with extractable metals explains total sediment C distribution across the floodplain better than POC, signifying the quantitative importance of mineral-organic associations for C storage within floodplain sediments.

Changing composition of mineral-organic associations across redox gradients

Detailed examination of the extractable metal pools yielded further insights into the impact of mineralogical composition on MAOC pools across the floodplain meander. Shallow sediments contained greater amounts of extractable Fe and Al compared to deep sediments (Fig. 4, $p < 0.05$), which predominantly reside in less extractable (HCl and dithionite) pools. Similarly, the relative abundance of HCl- and dithionite-extractable Fe and Al pools was significantly greater near the river than in the meander center (Fig. 4, $p < 0.05$; except dithionite-extractable Al: $p = 0.052$). The dominance of these pools in sediments at the surface and close to the river are suggestive of the formation and preservation of more crystalline Fe oxides phases in the oxic meander domains. In contrast, although the total extractable Fe concentrations declined toward the meander center, and total extractable Al remained constant, pyrophosphate-extractable Fe and Al concentrations increased towards the meander center, especially at depth (Fig. 4, $p < 0.05$). These results suggest that the more intense redox cycling in the meander center (Table S1) may have caused the loss of more crystalline Fe and Al phases but maintained a larger pool of short-range order Fe and Al phases that may be subject to repeated dissolution and precipitation

reactions. We suggest further research examine the impact of redox oscillations on the mobilization of reactive metal phases in floodplain sediments.

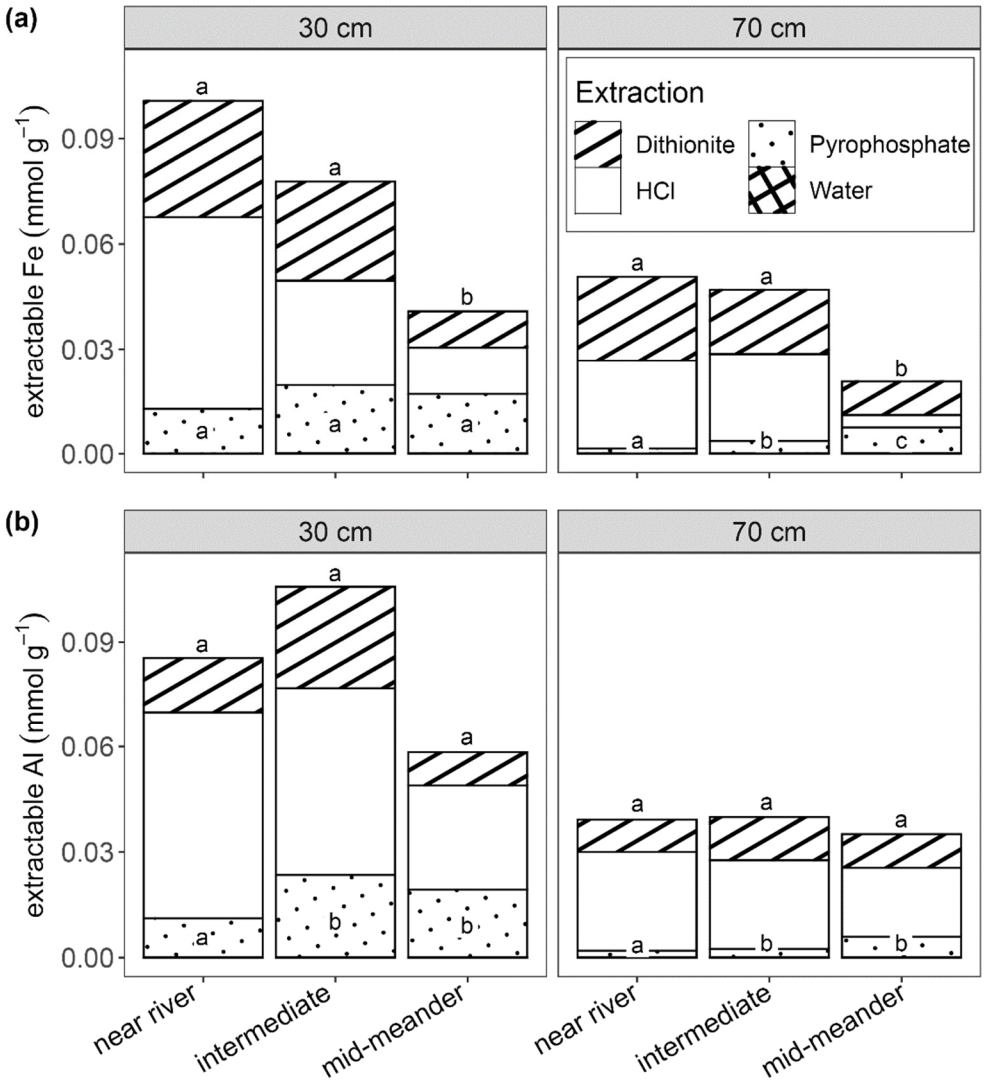

Figure 4: Composition of (a) extractable iron (Fe) and (b) extractable aluminum (Al) in shallow (30 cm) and deep (70 cm) sediment, across the floodplain meander. Extractable pools are denoted by pattern fills. Units for both panels are mmol metal per g sediment. Letter designations are Tukey's honestly significant difference test results ($p < 0.05$) based on differences along the meander in each depth: differences in total extractable Fe and pyrophosphate-extractable Fe in panel (a), and differences in total extractable Al and pyrophosphate-extractable Al in panel (b). Mean and standard errors are reported in Table S4 for extractable Fe and Table S5 for extractable Al.

In both surface and deep sediments, total extractable Fe decreased towards the meander center, whereas total extractable Al remained relatively constant across the meander (Fig. 4, $p <$

0.05). Consequently, the ratio of extractable Al/Fe increased by 93% from the near river position (0.82 ± 0.03) towards the meander center (1.58 ± 0.09, Fig. S3). These results suggest a relative enrichment of Al phases in the more reducing meander center, potentially due to loss of Fe oxides minerals via reductive dissolution ("gleying"). In deep sediments, while the pyrophosphate-extractable Al/Fe ratio decreased towards the meander center, the HCl-extractable Al/Fe ratio increased (Fig. S3). This result suggests that, at least in deep sediments, short-range order phases are relatively enriched in Fe, while relatively ordered phases are enriched in Al. Amorphous Al oxides have been shown to strongly sorb and thus protect OC [68], particularly in redox-active systems [32]. Notably, similar shifts from Fe- in oxic domains to Al-protected OC in anoxic domains have been observed in soils experiencing seasonal flooding [21,34,35] or contrasting precipitation [69].

Together, while the overall abundance of reactive Fe and Al phases declined towards the more redox-active meander center, we observed a relative increase in the abundance of water-extractable and pyrophosphate-extractable Fe and Al phases in comparison to the near river position. The greater abundance of such dissolved and short-range order Fe phases is likely a product of the more intense redox cycling that occurs here, which prevents formation of more crystalline phases due to repeated reduction cycles and export [70,71]. The concurrent decline in extractable Fe relative to Al suggests a redox-induced preferential loss of Fe phases and effective protection of remaining C within associations with Al phases. These results provide strong evidence for the role of redox dynamics in shaping the composition of mineral-organic associations in the sediments. However, it is important to acknowledge that there may have been differences in their original composition of mineral-organic associations upon deposition. While it was beyond the scope of this study, the question to what extent the composition of mineral-

organic associations in floodplain sediment is a function their original composition upon deposition versus subsequent biogeochemical transformations warrants further research.

Imprints of mineral versus anaerobic protection on organic matter composition

To assess variations in OC composition along the floodplain meander, we used high-resolution mass spectrometry (FT-ICR-MS) on our sequential extractions. Our results confirm our hypothesis that variable mineral characteristics and contrasting redox environments impact the composition of relatively accessible WEOC and less accessible MAOC pools. Across both depths, WEOC had significantly lower NOSC values and significantly higher molecular weights compared to other extracts (Fig. 5a and b, $p < 0.05$), suggesting that this relatively accessible OC has undergone less depolymerization and oxidation than OC protected within associations to minerals, potentially due to kinetic and thermodynamic constraints on its decomposition [18,19]. With each extraction step, the NOSC of extracted OC consistently increased while molecular weight decreased (Fig. 5a and b, $p < 0.05$). This result indicates that MAOC becomes more oxidized and depolymerized the less extractable (and presumably more ordered) the Fe and Al phases become. WEOC contains relatively more lipid-, amino sugar-, and protein-like compounds compared to MAOC (Fig. 5c), suggesting that WEOC is more microbial in nature (i.e., more microbial metabolites and extracellular enzymes) [72,73]. With each subsequent extraction step, the co-extracted OC becomes relatively more enriched in condensed hydrocarbon-, lignin-, and tannin-like compounds (Fig. 5c), suggesting that plant-derived aromatic compounds accumulate in association with increasingly stable Fe and Al oxides. These observations are consistent with evidence that low-molecular weight, oxidized, aromatic compounds preferentially bind to positively charged surfaces of Fe and Al oxides [43,45,74]. While

our results are supported in other studies, it is important to note that extraction conditions may alter SOM and thus impact downstream FT-ICR-MS analyses [75].

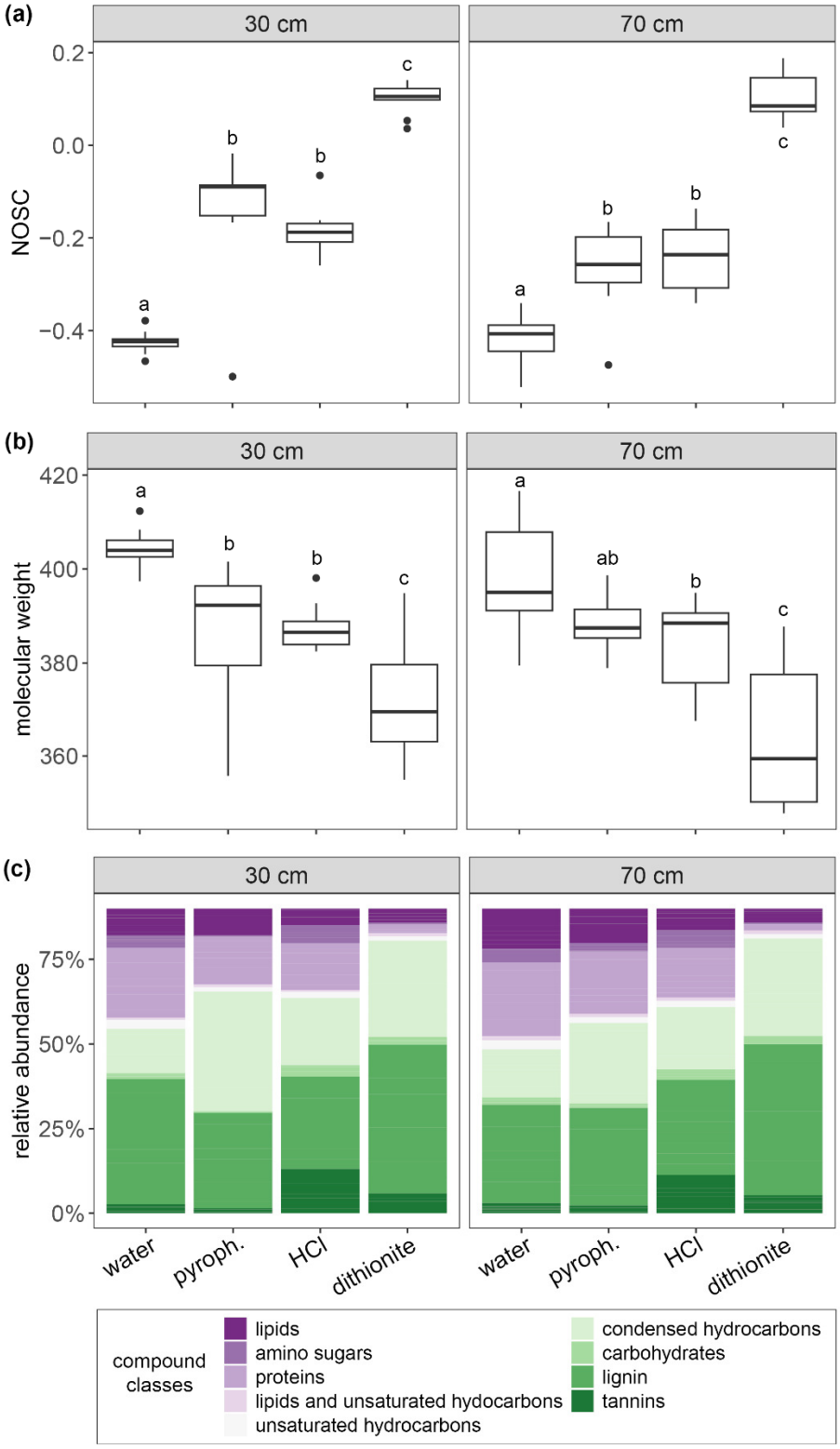

406 Figure 5: Composition of extracted organic matter in shallow (30 cm) and deep (70 cm) sediment: (a) nominal
407 oxidation state of carbon (NOSC), (b) molecular weight, and (c) compound classes by extractant (i.e., water,
408 pyrophosphate, HCl, and dithionite). Letter designations are Tukey's honestly significant difference test results ($p < 0.05$) based on differences across extractions in each depth.

410

411 We also found that the chemical composition of OC changed with sediment depth,
412 specifically in the pyrophosphate-extractable pool that accounted for the largest portion of
413 MAOC (Fig. 2b). As discussed above, OC co-extracted by pyrophosphate represents metal-
414 organic complexes, although it possibly also includes a significant fraction of base-extractable
415 OM [57] or nanocrystalline phases [67]. Compared to shallow sediments, pyrophosphate-extractable
416 OC in deep sediments consistently had lower NOSC (Fig. 5b) and aromaticity (double-bond
417 equivalence, DBE; aromaticity index, AI, Fig. S4), relatively more lipid-, amino sugar-, and
418 protein-like compounds (Fig. 5c), and a higher proportion of N-, P-, and S-containing
419 compounds (Fig. S5). Furthermore, sediment C/N ratios also decreased with depth, especially
420 towards the meander center (Fig. S6), which can be indicative of greater microbial processing
421 [45,76]. Together, these observations suggest that OC associated with amorphous metal complexes
422 in deep sediments may have a stronger microbial signature compared to shallow sediments.

423 While lower NOSC values at depth possibly indicate that anaerobic protection (i.e.,
424 kinetic and thermodynamic constraints) is a stronger control on OC storage in deeper sediments
425 than in shallow sediments, we did not find evidence that anaerobic protection becomes stronger
426 in the more reducing meander center. Rather than decline towards the more reduced meander
427 center, NOSC of pyrophosphate-extractable OC increased towards the center of the meander
428 (Fig. S7), albeit not significantly, suggesting a limited role for anaerobic protection in explaining
429 the observed OC accumulation in this pool (Fig. 2b). Because, as discussed above, MAOC (Fig.
430 2) and pyrophosphate-extractable metals (Fig. 4) increased towards the meander center, these

results indicate that mineral protection via metal-organic complexes, rather than solely anaerobic protection, drives OC accumulation patterns along this floodplain meander transect. In sum, these results suggest that mineral protection of OC in metal-organic complexes imprints on its composition in redox-dynamic floodplain sediments.

Dynamic nature of mineral-organic associations along floodplain meander

Storage of OC within floodplain sediments is often attributed to constraints on microbial metabolism under reducing conditions, with oxygen limitations restricting both oxidative depolymerization and aerobic respiration, thus protecting OC anaerobically. However, redox transitions experienced by hydrodynamic floodplain environments also impact mineral transformations, with relatively unknown consequences on the importance of mineral-organic associations in OC storage. Our detailed investigation of defined redox gradients emerging from textural variations and depth offers important insights on the quantitative importance and chemical nature of mineral-organic associations within floodplain sediments.

Overall, we found a strong correlation between total sediment C and different proxies for MAOC (isolated by density fractionation and sequential extraction), suggesting that mineral-organic associations contribute to OC storage within the sediments of this mountainous floodplain. The fact that extractable Fe and Al, rather than clay content, predicted OC content across the meander points to a critical role of Fe and Al oxides in the formation of mineral-organic associations within these floodplain sediments. While the importance of Fe and Al oxides for OC storage in upland soils[58] and even marine sediments[77] has long been established, our results support the notion that mineral protection, in addition to anaerobic protection, is also

453 critical for OC storage in floodplain sediments with high mineral content. This observations
454 contrasts with floodplains and wetland systems dominated by organic soils, such as peat-
455 dominated wetlands, where OC storage may be a consequence of anaerobic conditions[78], low
456 pH[42], or the inhibiting effects of phenolics[79].

457 Interestingly, the chemical nature of MAOC showed no significant spatial variations
458 across the meander but rather varied with crystallinity of the Fe and Al phases: with increasing
459 crystallinity, we saw greater contributions of oxidized, low-molecular weight, aromatic
460 compounds (Fig. 5). These results contrast with longer-term studies that examine the turnover of
461 OC[44,45], perhaps because of loss of more reactive short-range order phases in redox oscillating
462 soils over longer timescales. In contrast, the absolute amount of MAOC showed significant
463 spatial variations (Fig. 2). MAOC concentrations were greatest in the relatively oxic surface
464 horizons, coinciding with greater contents of less extractable, and presumably more ordered, Fe
465 and Al oxides (Fig. 4). In deeper sediments, despite the lower amounts of MAOC, the relative
466 contribution of MAOC to total sediment OC increased towards the more reducing meander
467 center (Fig. 2a). This increase in the apparent importance of mineral protection (relative to
468 anaerobic protection, as discussed above) in the meander center coincided with increases in the
469 OC pool bound in amorphous metal-organic complexes. This result suggests that while the
470 overall pool of extractable oxides declines (Fig. 4), a greater portion of the OC is sequestered in
471 short-range order or amorphous metal-organic complexes (Fig. 2b). Given the concurrent
472 increases in deep sediment clay content (Table 1) and pyrophosphate-extractable metals (Fig. 4),
473 it is possible that nano-particulate Fe/Al oxide phases or phyllosilicates may also play a role in
474 OC protection, although we did not directly measure phyllosilicate content.

475 Examination of the relative importance of mineral and anaerobic protection along redox
476 gradients within the floodplain sediments yielded unexpected results. We initially hypothesized
477 anaerobic protection to be most dominant in the more reduced meander sediments [19], resulting in
478 greater OC concentrations. Instead, sediment OC concentrations were significantly lower in the
479 fine-grained, reduced center of the meander and increased in the more oxic sediments near the
480 river (Fig. 2a). If burial and subsequent anaerobic protection on floodplain C solely explained the
481 C patterns along the floodplain meander, we further expected more relatively undegraded
482 particulate or reduced OC to accumulate to be more prevalent in the reduced meander center.
483 However, in the deep sediments, we found that POC declined towards the more reduced portion
484 of the meander, while water-extractable OC and NOSC remained relatively constant.
485 Conversely, we found that the relative contribution of MAOC increased towards the more
486 reduced center of the meander (Fig. 2). Together, these results suggest that the relative
487 importance of mineral protection increased towards the reduced meander center, while that of
488 anaerobic protection remained steady or diminished. While our study was qualitative in nature,
489 future studies should consider quantifying the contribution of mineral versus anaerobic
490 protection to floodplain sediment OC storage.

491 The prevalence of metal-organic complexes could be attributed to the fact that the
492 meander center experiences more dramatic and persistent reducing conditions with seasonal
493 flooding compared to sediments near the river (Table S1). Reducing conditions prompt reductive
494 Fe oxide dissolution and leaching of dissolved Fe from the system (i.e., gleying) [31,38], consistent
495 with the loss of extractable Fe (and Al) phases observed here. While the sediments become
496 reoxygenated every season, the oxidation-reduction cycles may be dramatic enough to prevent
497 formation of crystalline Fe oxides as has been observed in humid tropical soils that experience

redox heterogeneity due to frequent rainfall [38,80]. Instead, repeated oxidation-reduction cycles in response to flooding may only allowing for short-range order Fe (and Al) phases to form and persist [70,71]. Because those short-range order Fe phases are likely dissolved and re-precipitated during each oxidation-reduction cycles, their presence may indicate that MAOC within such metal-organic complexes may not be as protected as the MAOC bound to crystalline Fe and Al oxides within the more oxic meander sediments. It is also possible that redox cycling increases the formation of reactive oxygen species, which can also stimulate organic matter decomposition[81], and we suggest that further studies of carbon cycling in dynamic floodplains should incorporate this mechanism.

Environmental Implications

Together, our results support the notion that mineral-organic associations are more important for OC storage in redox active floodplain environments than previously recognized and may act in combination with anaerobic protection to limit OC export through microbial decomposition (as CO_2) and leaching (as DOC). Our results demonstrate that, depending on the redox regime, the quantitative importance of mineral protection as well as the chemical nature of mineral-organic associations controlling their stability vary across floodplain sediments. High elevation floodplains like that of the East River, CO, experience dynamic redox transitions with seasonal flooding events. The magnitude and timing of these seasonal flooding cycles is expected to change due to greater variability in snowpack[82], declines in snowpack depth [7,83], or slower snowmelt rates [84], which will directly impact the redox regime in the floodplains. Combined, our results suggest that such changes will not only directly affect anaerobic protection but may also have immediate consequences for protection in redox-sensitive mineral-organic associations,

521 warranting further exploration of potential impacts on OC storage within and export from
522 floodplain sediments.

523

524 **Author Contributions**

525 All authors contributed to the manuscript and have given approval to the final version of the
526 manuscript.

527 **Acknowledgments**

528 This research was supported by the Department of Energy, Office of Biological and
529 Environmental Research, Subsurface Biosphere Research program (grant no. DE-SC0016544). A
530 portion of the research was performed using EMSL, a DOE Office of Science User Facility
531 sponsored by the Office of Biological and Environmental Research. Field research was
532 conducted at the Rocky Mountain Biological Laboratory (Gothic, CO). XRF data were collected
533 at UC Riverside by Dr. Samantha Ying's research group. Texture analysis was conducted at
534 UMass Amherst with the assistance of Frances Griswold. Elsa Cousins assisted with the table of
535 contents graphic.

536

537 **Supporting Information**

538 East River discharge data; correlations between total sediment C and clay and extractable Ca;
539 extractable Al/Fe ratios; organic matter compositional differences; C/N ratios of mineral-
540 associated organic matter; water table depth, soil moisture, and soil redox potential across the
541 transect and over time; detailed sampling location information; means and standard errors for
542 extractable OC, Fe, and Al.

Data and Code Availability

The data used in this work will be available online at the ESS-DIVE database (https://ess-dive.lbl.gov/). Analysis code will be available on https://github.com/camganderson.

References

(1) D'Elia, A. H.; Liles, G. C.; Viers, J. H.; Smart, D. R. Deep Carbon Storage Potential of Buried Floodplain Soils. *Scientific Reports* **2017**, *7* (1). https://doi.org/10.1038/s41598-017-06494-4.

(2) Sutfin, N. A.; Wohl, E. Substantial Soil Organic Carbon Retention along Floodplains of Mountain Streams: Organic Carbon in Mountain Floodplains. *Journal of Geophysical Research: Earth Surface* **2017**, *122* (7), 1325–1338. https://doi.org/10.1002/2016JF004004.

(3) Sutfin, N. A.; Wohl, E. E.; Dwire, K. A. Banking Carbon: A Review of Organic Carbon Storage and Physical Factors Influencing Retention in Floodplains and Riparian Ecosystems. *Earth Surface Processes and Landforms* **2016**, *41* (1), 38–60. https://doi.org/10.1002/esp.3857.

(4) Battin, T. J.; Kaplan, L. A.; Findlay, S.; Hopkinson, C. S.; Marti, E.; Packman, A. I.; Newbold, J. D.; Sabater, F. Biophysical Controls on Organic Carbon Fluxes in Fluvial Networks. *Nature Geosci* **2008**, *1* (2), 95–100. https://doi.org/10.1038/ngeo101.

(5) Syvitski, J.; Ángel, J. R.; Saito, Y.; Overeem, I.; Vörösmarty, C. J.; Wang, H.; Olago, D. Earth's Sediment Cycle during the Anthropocene. *Nat Rev Earth Environ* **2022**. https://doi.org/10.1038/s43017-021-00253-w.

(6) Williams, A. P.; Cook, B. I.; Smerdon, J. E. Rapid Intensification of the Emerging Southwestern North American Megadrought in 2020–2021. *Nat. Clim. Chang.* **2022**, *12* (3), 232–234. https://doi.org/10.1038/s41558-022-01290-z.

(7) Siirila-Woodburn, E. R.; Rhoades, A. M.; Hatchett, B. J.; Huning, L. S.; Szinai, J.; Tague, C.; Nico, P. S.; Feldman, D. R.; Jones, A. D.; Collins, W. D.; Kaatz, L. A Low-to-No Snow Future and Its Impacts on Water Resources in the Western United States. *Nat Rev Earth Environ* **2021**, *2* (11), 800–819. https://doi.org/10.1038/s43017-021-00219-y.

(8) Wohl, E. An Integrative Conceptualization of Floodplain Storage. *Reviews of Geophysics* **2021**, *59* (2). https://doi.org/10.1029/2020RG000724.

(9) Wohl, E.; Pfeiffer, A. Organic Carbon Storage in Floodplain Soils of the U.S. Prairies. *River Research and Applications* **2018**. https://doi.org/10.1002/rra.3269.

(10) Chaopricha, N. T.; Marín-Spiotta, E. Soil Burial Contributes to Deep Soil Organic Carbon Storage. *Soil Biology and Biochemistry* **2014**, *69*, 251–264. https://doi.org/10.1016/j.soilbio.2013.11.011.

(11) Lininger, K. B.; Wohl, E.; Rose, J. R.; Leisz, S. J. Significant Floodplain Soil Organic Carbon Storage Along a Large High-Latitude River and Its Tributaries. *Geophys. Res. Lett.* **2019**, *46* (4), 2121–2129. https://doi.org/10.1029/2018GL080996.

(12) Mayer, S.; Schwindt, D.; Steffens, M.; Völkel, J.; Kögel-Knabner, I. Drivers of Organic Carbon Allocation in a Temperate Slope-Floodplain Catena under Agricultural Use. *Geoderma* **2018**, *327*, 63–72. https://doi.org/10.1016/j.geoderma.2018.04.021.

(13) Batson, J.; Noe, G. B.; Hupp, C. R.; Krauss, K. W.; Rybicki, N. B.; Schenk, E. R. Soil Greenhouse Gas Emissions and Carbon Budgeting in a Short-Hydroperiod Floodplain Wetland. *Journal of Geophysical Research: Biogeosciences* **2015**, *120* (1), 77–95.
(14) Gurwick, N. P.; McCorkle, D. M.; Groffman, P. M.; Gold, A. J.; Kellogg, D. Q.; Seitz-Rundlett, P. Mineralization of Ancient Carbon in the Subsurface of Riparian Forests. *J. Geophys. Res.* **2008**, *113* (G2), n/a-n/a. https://doi.org/10.1029/2007JG000482.
(15) Kroes, D. E.; Hupp, C. R. The Effect of Channelization on Floodplain Sediment Deposition and Subsidence Along the Pocomoke River, Maryland. *JAWRA Journal of the American Water Resources Association* **2010**, *46* (4), 686–699. https://doi.org/10.1111/j.1752-1688.2010.00440.x.
(16) Keiluweit, M.; Nico, P. S.; Kleber, M.; Fendorf, S. Are Oxygen Limitations under Recognized Regulators of Organic Carbon Turnover in Upland Soils? *Biogeochemistry* **2016**, *127* (2–3), 157–171. https://doi.org/10.1007/s10533-015-0180-6.
(17) Keiluweit, M.; Wanzek, T.; Kleber, M.; Nico, P.; Fendorf, S. Anaerobic Microsites Have an Unaccounted Role in Soil Carbon Stabilization. *Nat Commun* **2017**, *8* (1), 1771. https://doi.org/10.1038/s41467-017-01406-6.
(18) Naughton, H. R.; Keiluweit, M.; Tfaily, M. M.; Dynes, J. J.; Regier, T.; Fendorf, S. Development of Energetic and Enzymatic Limitations on Microbial Carbon Cycling in Soils. *Biogeochemistry* **2021**, *153* (2), 191–213. https://doi.org/10.1007/s10533-021-00781-z.
(19) Boye, K.; Noël, V.; Tfaily, M. M.; Bone, S. E.; Williams, K. H.; Bargar, J. R.; Fendorf, S. Thermodynamically Controlled Preservation of Organic Carbon in Floodplains. *Nature Geoscience* **2017**. https://doi.org/10.1038/ngeo2940.
(20) Lacroix, E. M.; Rossi, R. J.; Bossio, D.; Fendorf, S. Effects of Moisture and Physical Disturbance on Pore-Scale Oxygen Content and Anaerobic Metabolisms in Upland Soils. *Science of The Total Environment* **2021**, *780*, 146572. https://doi.org/10.1016/j.scitotenv.2021.146572.
(21) LaCroix, R. E.; Tfaily, M. M.; McCreight, M.; Jones, M. E.; Spokas, L.; Keiluweit, M. Shifting Mineral and Redox Controls on Carbon Cycling in Seasonally Flooded Mineral Soils. *Biogeosciences* **2019**, *16* (13), 2573–2589. https://doi.org/10.5194/bg-16-2573-2019.
(22) LaRowe, D. E.; Van Cappellen, P. Degradation of Natural Organic Matter: A Thermodynamic Analysis. *Geochimica et Cosmochimica Acta* **2011**, *75* (8), 2030–2042. https://doi.org/10.1016/j.gca.2011.01.020.
(23) Mikutta, R.; Mikutta, C.; Kalbitz, K.; Scheel, T.; Kaiser, K.; Jahn, R. Biodegradation of Forest Floor Organic Matter Bound to Minerals via Different Binding Mechanisms. *Geochimica et Cosmochimica Acta* **2007**, *71* (10), 2569–2590. https://doi.org/10.1016/j.gca.2007.03.002.
(24) Porras, R. C.; Hicks Pries, C. E.; McFarlane, K. J.; Hanson, P. J.; Torn, M. S. Association with Pedogenic Iron and Aluminum: Effects on Soil Organic Carbon Storage and Stability in Four Temperate Forest Soils. *Biogeochemistry* **2017**. https://doi.org/10.1007/s10533-017-0337-6.
(25) Torn, M. S.; Trumbore, S. E.; Chadwick, O. A.; Vitousek, P. M.; Hendricks, D. M. Mineral Control of Soil Organic Carbon Storage and Turnover. *Nature* **1997**, *389* (6647), 170–173.
(26) Kleber, M.; Eusterhues, K.; Keiluweit, M.; Mikutta, C.; Mikutta, R.; Nico, P. S. Mineral–Organic Associations: Formation, Properties, and Relevance in Soil Environments. In *Advances in Agronomy*; Elsevier, 2015; Vol. 130, pp 1–140. https://doi.org/10.1016/bs.agron.2014.10.005.
(27) Kleber, M.; Bourg, I. C.; Coward, E. K.; Hansel, C. M.; Myneni, S. C. B.; Nunan, N. Dynamic Interactions at the Mineral–Organic Matter Interface. *Nat Rev Earth Environ* **2021**. https://doi.org/10.1038/s43017-021-00162-y.
(28) Coward, E. K.; Thompson, A. T.; Plante, A. F. Iron-Mediated Mineralogical Control of Organic Matter Accumulation in Tropical Soils. *Geoderma* **2017**, *306*, 206–216. https://doi.org/10.1016/j.geoderma.2017.07.026.

(29) Kirsten, M.; Mikutta, R.; Vogel, C.; Thompson, A.; Mueller, C. W.; Kimaro, D. N.; Bergsma, H. L. T.; Feger, K.-H.; Kalbitz, K. Iron Oxides and Aluminous Clays Selectively Control Soil Carbon Storage and Stability in the Humid Tropics. *Sci Rep* **2021**, *11* (1), 5076. https://doi.org/10.1038/s41598-021-84777-7.

(30) Rasmussen, C.; Heckman, K.; Wieder, W. R.; Keiluweit, M.; Lawrence, C. R.; Berhe, A. A.; Blankinship, J. C.; Crow, S. E.; Druhan, J. L.; Hicks Pries, C. E.; Marin-Spiotta, E.; Plante, A. F.; Schädel, C.; Schimel, J. P.; Sierra, C. A.; Thompson, A.; Wagai, R. Beyond Clay: Towards an Improved Set of Variables for Predicting Soil Organic Matter Content. *Biogeochemistry* **2018**. https://doi.org/10.1007/s10533-018-0424-3.

(31) Chen, C.; Kukkadapu, R. K.; Lazareva, O.; Sparks, D. L. Solid-Phase Fe Speciation along the Vertical Redox Gradients in Floodplains Using XAS and Mössbauer Spectroscopies. *Environmental Science & Technology* **2017**, *51* (14), 7903–7912. https://doi.org/10.1021/acs.est.7b00700.

(32) Darke, A. K.; Walbridge, M. R. Al and Fe Biogeochemistry in a Floodplain Forest: Implications for P Retention. *Biogeochemistry* **2000**, 32.

(33) Anthony, T. L.; Silver, W. L. Mineralogical Associations with Soil Carbon in Managed Wetland Soils. *Global Change Biology* **2020**, *26* (11), 6555–6567. https://doi.org/10.1111/gcb.15309.

(34) Nitzsche, K. N.; Kayler, Z. E.; Premke, K.; Gessler, A.; Wagai, R. Divergent Roles of Iron and Aluminum in Sediment Organic Matter Association at the Terrestrial–Aquatic Interface. *Biogeochemistry* **2022**. https://doi.org/10.1007/s10533-021-00878-5.

(35) Possinger, A. R.; Bailey, S. W.; Inagaki, T. M.; Kögel-Knabner, I.; Dynes, J. J.; Arthur, Z. A.; Lehmann, J. Organo-Mineral Interactions and Soil Carbon Mineralizability with Variable Saturation Cycle Frequency. *Geoderma* **2020**, *375*, 114483. https://doi.org/10.1016/j.geoderma.2020.114483.

(36) Adhikari, D.; Zhao, Q.; Das, K.; Mejia, J.; Huang, R.; Wang, X.; Poulson, S. R.; Tang, Y.; Roden, E. E.; Yang, Y. Dynamics of Ferrihydrite-Bound Organic Carbon during Microbial Fe Reduction. *Geochimica et Cosmochimica Acta* **2017**, *212*, 221–233. https://doi.org/10.1016/j.gca.2017.06.017.

(37) Bhattacharyya, A.; Schmidt, M. P.; Stavitski, E.; Martínez, C. E. Iron Speciation in Peats: Chemical and Spectroscopic Evidence for the Co-Occurrence of Ferric and Ferrous Iron in Organic Complexes and Mineral Precipitates. *Organic Geochemistry* **2017**. https://doi.org/10.1016/j.orggeochem.2017.10.012.

(38) Bhattacharyya, A.; Campbell, A. N.; Tfaily, M. M.; Lin, Y.; Kukkadapu, R. K.; Silver, W. L.; Nico, P. S.; Pett-Ridge, J. Redox Fluctuations Control the Coupled Cycling of Iron and Carbon in Tropical Forest Soils. *Environ. Sci. Technol.* **2018**, *52* (24), 14129–14139. https://doi.org/10.1021/acs.est.8b03408.

(39) Tishchenko, V.; Meile, C.; Scherer, M. M.; Pasakarnis, T. S.; Thompson, A. Fe 2+ Catalyzed Iron Atom Exchange and Re-Crystallization in a Tropical Soil. *Geochimica et Cosmochimica Acta* **2015**, *148*, 191–202. https://doi.org/10.1016/j.gca.2014.09.018.

(40) Das, S.; Richards, B. K.; Hanley, K. L.; Krounbi, L.; Walter, M. F.; Walter, M. T.; Steenhuis, T. S.; Lehmann, J. Lower Mineralizability of Soil Carbon with Higher Legacy Soil Moisture. *Soil Biology and Biochemistry* **2019**, *130*, 94–104. https://doi.org/10.1016/j.soilbio.2018.12.006.

(41) Kang, H.; Kwon, M. J.; Kim, S.; Lee, S.; Jones, T. G.; Johncock, A. C.; Haraguchi, A.; Freeman, C. Biologically Driven DOC Release from Peatlands during Recovery from Acidification. *Nat Commun* **2018**, *9* (1), 3807. https://doi.org/10.1038/s41467-018-06259-1.

(42) Ye, R.; Jin, Q.; Bohannan, B.; Keller, J. K.; McAllister, S. A.; Bridgham, S. D. PH Controls over Anaerobic Carbon Mineralization, the Efficiency of Methane Production, and Methanogenic Pathways in Peatlands across an Ombrotrophic–Minerotrophic Gradient. *Soil Biology and Biochemistry* **2012**, *54*, 36–47. https://doi.org/10.1016/j.soilbio.2012.05.015.

(43) Coward, E. K.; Ohno, T.; Plante, A. F. Adsorption and Molecular Fractionation of Dissolved Organic Matter on Iron-Bearing Mineral Matrices of Varying Crystallinity. *Environmental Science & Technology* **2018**, *52* (3), 1036–1044. https://doi.org/10.1021/acs.est.7b04953.

(44) Hall, S. J.; Berhe, A. A.; Thompson, A. Order from Disorder: Do Soil Organic Matter Composition and Turnover Co-Vary with Iron Phase Crystallinity? *Biogeochemistry* **2018**, *140* (1), 93–110. https://doi.org/10.1007/s10533-018-0476-4.
(45) Kramer, M. G.; Sanderman, J.; Chadwick, O. A.; Chorover, J.; Vitousek, P. M. Long-Term Carbon Storage through Retention of Dissolved Aromatic Acids by Reactive Particles in Soil. *Global Change Biology* **2012**, *18* (8), 2594–2605. https://doi.org/10.1111/j.1365-2486.2012.02681.x.
(46) Bhattacharyya, A.; Kukkadapu, R. K.; Bowden, M.; Pett-Ridge, J.; Nico, P. S. Fast Redox Switches Lead to Rapid Transformation of Goethite in Humid Tropical Soils: A Mössbauer Spectroscopy Study. *Soil Science Soc of Amer J* **2022**, *86* (2), 264–274. https://doi.org/10.1002/saj2.20382.
(47) Thompson, A.; Chadwick, O. A.; Rancourt, D. G.; Chorover, J. Iron-Oxide Crystallinity Increases during Soil Redox Oscillations. *Geochimica et Cosmochimica Acta* **2006**, *70* (7), 1710–1727. https://doi.org/10.1016/j.gca.2005.12.005.
(48) Hubbard, S. S.; Williams, K. H.; Agarwal, D.; Banfield, J.; Beller, H.; Bouskill, N.; Brodie, E.; Carroll, R.; Dafflon, B.; Dwivedi, D.; Falco, N.; Faybishenko, B.; Maxwell, R.; Nico, P.; Steefel, C.; Steltzer, H.; Tokunaga, T.; Tran, P. A.; Wainwright, H.; Varadharajan, C. The East River, Colorado, Watershed: A Mountainous Community Testbed for Improving Predictive Understanding of Multiscale Hydrological–Biogeochemical Dynamics. *Vadose Zone Journal* **2018**, *17* (1), 0. https://doi.org/10.2136/vzj2018.03.0061.
(49) Dong, W.; Bhattacharyya, A.; Fox, P. M.; Bill, M.; Dwivedi, D.; Carrero, S.; Conrad, M.; Nico, P. S. Geochemical Controls on Release and Speciation of Fe(II) and Mn(II) From Hyporheic Sediments of East River, Colorado. *Front. Water* **2020**, *2*, 562298. https://doi.org/10.3389/frwa.2020.562298.
(50) Dwivedi, D.; Steefel, C. I.; Arora, B.; Newcomer, M.; Moulton, J. D.; Dafflon, B.; Faybishenko, B.; Fox, P.; Nico, P.; Spycher, N.; Carroll, R.; Williams, K. H. Geochemical Exports to River From the Intrameander Hyporheic Zone Under Transient Hydrologic Conditions: East River Mountainous Watershed, Colorado. *Water Resources Research* **2018**, *54* (10), 8456–8477. https://doi.org/10.1029/2018WR023377.
(51) Fox, P. M.; Bill, M.; Heckman, K.; Conrad, M.; Anderson, C.; Keiluweit, M.; Nico, P. S. Shale as a Source of Organic Carbon in Floodplain Sediments of a Mountainous Watershed. *J. Geophys. Res. Biogeosci.* **2020**, *125* (2). https://doi.org/10.1029/2019JG005419.
(52) Falco, N.; Wainwright, H.; Dafflon, B.; Léger, E.; Peterson, J.; Steltzer, H.; Wilmer, C.; Rowland, J. C.; Williams, K. H.; Hubbard, S. S. Investigating Microtopographic and Soil Controls on a Mountainous Meadow Plant Community Using High-Resolution Remote Sensing and Surface Geophysical Data. *J. Geophys. Res. Biogeosci.* **2019**, *124* (6), 1618–1636. https://doi.org/10.1029/2018JG004394.
(53) Dafflon, B.; Dwivedi, D. Groundwater Level Elevation and Temperature at the Lower Montane in the East River Watershed, Colorado, 2020. doi:10.15485/1647040 (accessed 2022-11-25).
(54) Keiluweit, M.; Gee, K.; Denney, A.; Fendorf, S. Anoxic Microsites in Upland Soils Dominantly Controlled by Clay Content. *Soil Biology and Biochemistry* **2018**, *118*, 42–50. https://doi.org/10.1016/j.soilbio.2017.12.002.
(55) Hatton, P.-J.; Kleber, M.; Zeller, B.; Moni, C.; Plante, A. F.; Townsend, K.; Gelhaye, L.; Lajtha, K.; Derrien, D. Transfer of Litter-Derived N to Soil Mineral–Organic Associations: Evidence from Decadal 15N Tracer Experiments. *Organic Geochemistry* **2012**, *42* (12), 1489–1501. https://doi.org/10.1016/j.orggeochem.2011.05.002.
(56) Fox, P. M.; Nico, P. S.; Tfaily, M. M.; Heckman, K.; Davis, J. A. Characterization of Natural Organic Matter in Low-Carbon Sediments: Extraction and Analytical Approaches. *Organic Geochemistry* **2017**. https://doi.org/10.1016/j.orggeochem.2017.08.009.
(57) Heckman, K.; Lawrence, C. R.; Harden, J. W. A Sequential Selective Dissolution Method to Quantify Storage and Stability of Organic Carbon Associated with Al and Fe Hydroxide Phases. *Geoderma* **2018**, *312*, 24–35. https://doi.org/10.1016/j.geoderma.2017.09.043.

(58) Wagai, R.; Mayer, L. M. Sorptive Stabilization of Organic Matter in Soils by Hydrous Iron Oxides. *Geochimica et Cosmochimica Acta* **2007**, *71* (1), 25–35. https://doi.org/10.1016/j.gca.2006.08.047.
(59) Kaiser, M.; Zederer, D. P.; Ellerbrock, R. H.; Sommer, M.; Ludwig, B. Effects of Mineral Characteristics on Content, Composition, and Stability of Organic Matter Fractions Separated from Seven Forest Topsoils of Different Pedogenesis. *Geoderma* **2016**, *263*, 1–7. https://doi.org/10.1016/j.geoderma.2015.08.029.
(60) Dittmar, T.; Koch, B.; Hertkorn, N.; Kattner, G. A Simple and Efficient Method for the Solid-Phase Extraction of Dissolved Organic Matter (SPE-DOM) from Seawater. *Limnology and Oceanography: Methods* **2008**, *6* (6), 230–235.
(61) Tolić, N.; Liu, Y.; Liyu, A.; Shen, Y.; Tfaily, M. M.; Kujawinski, E. B.; Longnecker, K.; Kuo, L.-J.; Robinson, E. W.; Paša-Tolić, L.; others. Formularity: Software for Automated Formula Assignment of Natural and Other Organic Matter from Ultrahigh-Resolution Mass Spectra. *Analytical chemistry* **2017**, *89* (23), 12659–12665.
(62) Tfaily, M. M.; Hess, N. J.; Koyama, A.; Evans, R. Elevated [CO2] Changes Soil Organic Matter Composition and Substrate Diversity in an Arid Ecosystem. *Geoderma* **2018**, *330*, 1–8.
(63) Bailey, V. L.; Smith, A. P.; Tfaily, M.; Fansler, S. J.; Bond-Lamberty, B. Differences in Soluble Organic Carbon Chemistry in Pore Waters Sampled from Different Pore Size Domains. *Soil Biology and Biochemistry* **2017**, *107*, 133–143. https://doi.org/10.1016/j.soilbio.2016.11.025.
(64) R Core Team. *R: A Language and Environment for Statistical Computing*; R Foundation for Statistical Computing: Vienna, Austria, 2022.
(65) Mendiburu, F. de; Yaseen, M. *Agricolae: Statistical Procedures for Agricultural Research*; 2021.
(66) Wagai, R.; Mayer, L. M.; Kitayama, K.; Shirato, Y. Association of Organic Matter with Iron and Aluminum across a Range of Soils Determined via Selective Dissolution Techniques Coupled with Dissolved Nitrogen Analysis. *Biogeochemistry* **2013**, *112* (1–3), 95–109. https://doi.org/10.1007/s10533-011-9652-5.
(67) Regelink, I. C.; Voegelin, A.; Weng, L.; Koopmans, G. F.; Comans, R. N. J. Characterization of Colloidal Fe from Soils Using Field-Flow Fractionation and Fe K-Edge X-Ray Absorption Spectroscopy. *Environ. Sci. Technol.* **2014**, *48* (8), 4307–4316. https://doi.org/10.1021/es405330x.
(68) Schneider, M. P. W.; Scheel, T.; Mikutta, R.; van Hees, P.; Kaiser, K.; Kalbitz, K. Sorptive Stabilization of Organic Matter by Amorphous Al Hydroxide. *Geochimica et Cosmochimica Acta* **2010**, *74* (5), 1606–1619. https://doi.org/10.1016/j.gca.2009.12.017.
(69) Inagaki, T. M.; Possinger, A. R.; Grant, K. E.; Schweizer, S. A.; Mueller, C. W.; Derry, L. A.; Lehmann, J.; Kögel-Knabner, I. Subsoil Organo-Mineral Associations under Contrasting Climate Conditions. *Geochimica et Cosmochimica Acta* **2020**, *270*, 244–263. https://doi.org/10.1016/j.gca.2019.11.030.
(70) Ginn, B.; Meile, C.; Wilmoth, J.; Tang, Y.; Thompson, A. Rapid Iron Reduction Rates Are Stimulated by High-Amplitude Redox Fluctuations in a Tropical Forest Soil. *Environmental Science & Technology* **2017**, *51* (6), 3250–3259. https://doi.org/10.1021/acs.est.6b05709.
(71) Winkler, P.; Kaiser, K.; Thompson, A.; Kalbitz, K.; Fiedler, S.; Jahn, R. Contrasting Evolution of Iron Phase Composition in Soils Exposed to Redox Fluctuations. *Geochimica et Cosmochimica Acta* **2018**, *235*, 89–102. https://doi.org/10.1016/j.gca.2018.05.019.
(72) Guigue, J.; Harir, M.; Mathieu, O.; Lucio, M.; Ranjard, L.; Lévêque, J.; Schmitt-Kopplin, P. Ultrahigh-Resolution FT-ICR Mass Spectrometry for Molecular Characterisation of Pressurised Hot Water-Extractable Organic Matter in Soils. *Biogeochemistry* **2016**, *128* (3), 307–326. https://doi.org/10.1007/s10533-016-0209-5.
(73) Malik, A. A.; Roth, V.-N.; Hébert, M.; Tremblay, L.; Dittmar, T.; Gleixner, G. Linking Molecular Size, Composition and Carbon Turnover of Extractable Soil Microbial Compounds. *Soil Biology and Biochemistry* **2016**, *100*, 66–73. https://doi.org/10.1016/j.soilbio.2016.05.019.

(74) Possinger, A. R.; Zachman, M. J.; Enders, A.; Levin, B. D. A.; Muller, D. A.; Kourkoutis, L. F.; Lehmann, J. Organo–Organic and Organo–Mineral Interfaces in Soil at the Nanometer Scale. *Nat Commun* **2020**, *11* (1), 6103. https://doi.org/10.1038/s41467-020-19792-9.
(75) Lv, J.; Huang, Z.; Christie, P.; Zhang, S. Reducing Reagents Induce Molecular Artifacts in the Extraction of Soil Organic Matter. *ACS Earth Space Chem.* **2020**, *4* (11), 1913–1919. https://doi.org/10.1021/acsearthspacechem.0c00194.
(76) Wang, B.; An, S.; Liang, C.; Liu, Y.; Kuzyakov, Y. Microbial Necromass as the Source of Soil Organic Carbon in Global Ecosystems. *Soil Biology and Biochemistry* **2021**, *162*, 108422. https://doi.org/10.1016/j.soilbio.2021.108422.
(77) Lalonde, K.; Mucci, A.; Ouellet, A.; Gélinas, Y. Preservation of Organic Matter in Sediments Promoted by Iron. *Nature* **2012**, *483* (7388), 198–200. https://doi.org/10.1038/nature10855.
(78) Wilmoth, J. L.; Schaefer, J. K.; Schlesinger, D. R.; Roth, S. W.; Hatcher, P. G.; Shoemaker, J. K.; Zhang, X. The Role of Oxygen in Stimulating Methane Production in Wetlands. *Glob Change Biol* **2021**, gcb.15831. https://doi.org/10.1111/gcb.15831.
(79) Fenner, N.; Freeman, C. Woody Litter Protects Peat Carbon Stocks during Drought. *Nat. Clim. Chang.* **2020**, *10* (4), 363–369. https://doi.org/10.1038/s41558-020-0727-y.
(80) Chen, C.; Meile, C.; Wilmoth, J.; Barcellos, D.; Thompson, A. Influence of PO_2 on Iron Redox Cycling and Anaerobic Organic Carbon Mineralization in a Humid Tropical Forest Soil. *Environmental Science & Technology* **2018**, *52* (14), 7709–7719. https://doi.org/10.1021/acs.est.8b01368.
(81) Hall, S. J.; Silver, W. L. Iron Oxidation Stimulates Organic Matter Decomposition in Humid Tropical Forest Soils. *Global Change Biology* **2013**, *19* (9), 2804–2813. https://doi.org/10.1111/gcb.12229.
(82) Lute, A. C.; Abatzoglou, J. T.; Hegewisch, K. C. Projected Changes in Snowfall Extremes and Interannual Variability of Snowfall in the Western United States. *Water Resour. Res.* **2015**, *51* (2), 960–972. https://doi.org/10.1002/2014WR016267.
(83) Fyfe, J. C.; Derksen, C.; Mudryk, L.; Flato, G. M.; Santer, B. D.; Swart, N. C.; Molotch, N. P.; Zhang, X.; Wan, H.; Arora, V. K.; Scinocca, J.; Jiao, Y. Large Near-Term Projected Snowpack Loss over the Western United States. *Nat Commun* **2017**, *8* (1), 14996. https://doi.org/10.1038/ncomms14996.
(84) Musselman, K. N.; Addor, N.; Vano, J. A.; Molotch, N. P. Winter Melt Trends Portend Widespread Declines in Snow Water Resources. *Nat. Clim. Chang.* **2021**, *11* (5), 418–424. https://doi.org/10.1038/s41558-021-01014-9.